LASER TRAPPING IONIZATION OF HUMAN RED BLOOD CELLS WITH FOUR HEMOGLOBIN TYPES: A PRELIMINARY STUDY OF HEMOGLOBIN QUANTITATION

A THESIS SUBMITTED TO THE DEPARTMENT OF PHYSICS PRESENTED IN PARTIAL FULFILLMENT OF THE REQUIREMENTS FOR THE DEGREE OF MASTER OF SCIENCE (PHYSICS)

M.Sc. Thesis

Addis Ababa University
School of Graduate Studies

Deresse Ahmed Adem
Addis Ababa, Ethiopia
July 2017

Addis Ababa University
School of Graduate Studies
College of Natural Sciences
Faculty of Chemical and Physical Sciences
Department of Physics

The undersigned here by certify that they have read and recommend to the School of Graduate Studies for acceptance a thesis entitled "**LASER TRAPPING IONIZATION OF HUMAN RED BLOOD CELLS WITH FOUR HEMOGLOBIN TYPES: A PRELIMINARY STUDY OF HEMOGLOBIN QUANTITATION** " by **Deresse Ahmed Adem** in partial fulfillment of the requirements for the degree of **Master of Science in Physics**.

Dated: July 2017

Approved by the Examination Committee:

Prof. Daniel Erenso, Advisor ———————————

Prof. Gholap Ashok, Examiner ———————————

Dr. Tesfaye Kidane, Examiner ———————————

ADDIS ABABA UNIVERSITY

Date: **July 2017**

Author: **Deresse Ahmed Adem**

Title: **LASER TRAPPING IONIZATION OF HUMAN RED BLOOD CELLS WITH FOUR HEMOGLOBIN TYPES: A PRELIMINARY STUDY OF HEMOGLOBIN QUANTITATION**

Department: **Physics**

Degree: **M.Sc.** Convocation: **June** Year: **2017**

Permission is herewith granted to Addis Ababa University to circulate and to have copied for non-commercial purposes, at its discretion, the above title upon the request of individuals or institutions.

Signature of Author

Table of Contents

List of Figures

Abstract

In this work, a high intensity gradient laser was used to study the threshold ionization energy, the threshold radiation dose, and the charge (to determine hemoglobin quantitation) of four different samples of hemoglobin type. The study was conducted using AS, AC, FA or AF, and FSC hemoglobin types were obtained from MSCC at the MMC. The experiment was performed for each cell, for a total of 62 cells for Hb AS, Hb FA, and Hb FSC, and 47 cells for Hb AC, were trapped and ionized by a high intensity infrared laser at 1064 nm. With the laser trap serving as a radiation source, the cell underwent dielectric breakdown of the membrane. When this process occurs, the cell becomes highly charged and its dielectric susceptibility changes. The charge creates an increasing electrostatic force while the changing dielectric susceptibility diminishes the strength of the trapping force. Consequently, at some instant of time the cell gets ejected from the trap. The time inside the trap (ionization time) while the cell is being ionized is used to determine the threshold ionization energy and threshold radiation dose, and the intensity of radiation and the post ionization trajectory of the cells are used to determine the the charge for each cell of four different samples of hemoglobin type using NonlinearModelFit in Mathematica. Laser tapping technique is indeeded promissing for a very precise measurement of the hemoglobin types present in a blood sample. Knowing the hemodlobin type present in a blood sample is essential in screening sickle cell diseases and will vastly improve the accuracy of monitoring a sickle cell anemia patients receiving various types of treatments,

Acknowledgements

First of all, I would like to thank almighty God who made it possible, to begin and finish this work successfully. I would like to express my sincere gratitude to Prof. Daniel Erenso, my research advisor for admitting me into the Experimental Biomedical Optics program, and for his never failing suggestions, advice, guidance, patience, and constant encouragement helped me to complete the present thesis work successfully. He is the person who has always helped me as friendly approach and fatherhood advice. I have learned a lot not only in the physics part but also to be kind, patient, respectful and to have confidence in my work. This experience has made a great deal of difference to my development as a physics student. I am very grateful once again to him for all the things he has done for me.

Words can not express my felling which I have for my mother Neimu Muhye, my father Ahmed Adem and whole family. I am highly indebted to them for their blessing, guidance, advice, encouragement.

I am eternally grateful to Dr. Teshome Senbeta (Addis Ababa University chairman of Department of Physics) and Dr. Deribe Hirpo (my instructor) for their patience and constant help throughout my learning process and research, words are not enough, only eternal gratitude. I would also like to thank Statistical and Computational Physics graduate students, Mr. Tibebe Birhanu, Mr. Yigermal Bassie and Mr. Yoseph Abebe for their suggestions.

Finally I would like to thank the department of physics and school of graduate studies of Addis Ababa University and Wolkite University for all support I got during my study.

I would like to dedicate my thesis in the memory of my uncle Mr. Ali Muhye, Mr. Muhye Adem and my aunt Ms.Tsehay Muhye.

Acronyms

ATCC - American Type Culture Collection

BE- Beam Expander

DM - Dichroic Mirror

FBS - Fatal Bovine Serum

Hb - Hemoglobin

HPLC - High Performance Liquid Chramatography

LT - Laser Trapping

MTSU - Middle Tenesse State University

MSCC - Meharry Sickle Cell Center

MMC - Meharry Medical Center

OL - Objective Lens

RBCs - Red Blood Cells

SCT - Sickle Cell Trait

SCD - Sickle Cell Disease

TIE - Threshold Ionization Energy

TRD - Threshold Radiation Dose

Chapter 1

Introduction

High performance liquid chromatography (HPLC) is commonly used to determine the relative percentage of the hemoglobin types present in a blood sample[1]. Hb quantitation in a blood sample is essential in screening Hb disorder such as SCD and also in monitoring patients receiving various types of treatments. HPLC techniques employ principles of ion exchange chromatography and spectrophotometric detection. In this technique a few microliters of blood is hemolyzed and injected onto a positively charged column of HPLC. At a moderately alkaline pH, all hemoglobin types carry a variable net negative charge and bind with the positively charged column. However, the magnitude of the negative charge varies from one type of hemoglobin to another. Although there are many types of hemoglobin, the most common hemoglobin types found in blood are F, A, S, and C. In this order Hb F has the weakest and Hb C has the strongest negative charge. When these different Hb types are injected into the positively charged HPLC column, the Hb F type will bind weakly and be eluted quickly from the column whereas the Hb C type will bind more strongly and be retained longer on the column[2 - 4]. The work we present here is motivated by an interest in further application of a recently introduced new approach for charge quantitation by single cell ionization. This new approach uses LT techniques to trap and ionized single cell in order to determine the threshold ionization energy and the resulting charge. LT techniques have long been used to study the elastic properties of human red blood cells [4]. However, it has never been used as an alternative techniques for Hb quantitation in blood sample.

A software program is used to analyze the data collected from the biomedical optics lab at MTSU. We have used Image Pro. 6.2 software program to measure the mean diameter of the each cell before the cell is trapped, to determine the ionization time when the cell is in side the trap, and to measure the trajectory of each cell after the cell is ejected from the trap. In addition to Image Pro. 6.2 software program we have used graphical and statistical analysis software, Origin Lab 2015 and Wolfram Mathematica 9 software. We have used graphical and statistical analysis software, Origin Lab 2015, to plot graphs such as displacement vs time graphs, the statistical data distribution of the TIE and TRD and the statistical data distribution of the charge in z number and z number per unit area as a function of the mean diameter and to carried out statistically valid data reduction for high standard deviation. We have used Wolfram Mathematica 9 software to determine the charge of each cell and the stiffness of the trapping force by fitting the theoretical model with the experimental data that we use for this study.

Chapter 2

Background theory

In this chapter we will discuss about the basic concept of optical trapping, working principle of optical tweezer and its application in biophysics for cell manipulation. This chapter is organized in sub-topics such as laser trap fundamentals, physical principle of optical tweezers, force affecting the trapped particles and modeling optical trapping forces.

2.1 Optical Trapping History

In 1871 Maxwell theorized that the momentum of light could exert a pressure on a surface, an effect that was later called "radiation pressure" [5]. Lebedev, and independently, Nichols and Hull experimentally demonstrated that light could exert a pressure on an object in 1901 [6, 7]. This pressure was very weak as there was a low photon flux. A large increase in the photon flux was achieved with the invention of the laser in 1960, and with this increase in photon flux it was realized that radiation pressure could be used to perform tasks. In 1971 Ashkin *et al* use the forces of radiation pressure from laser light to trap a 20μm dielectric particle [8]. Ashkin, among others, continued working in the field of optically trapping particles and published several articles regarding atom and colloidal particle trapping [9 - 12]. This work later split into two categories: laser atom cooling and optical trapping. In 1986 Ashkin *et al* reported the first use of a single-beam optical trap to hold particles between 25 nm and 10μm in diameter at a fixed point in water. Shortly after this publication the apparatus that Ashkin used to trap these particles became known as optical tweezers and the method known as optical trapping [13]. Today optical tweezers are used in a variety of ways. In the biological and medicinal sciences optical tweezers are often used to separate different cell types, manipulate sub cellular objects without damaging the cell itself and for medicinal procedures such as invitro fertilisation. Most

commercial optical tweezers are aimed at the biological and medical markets and, as such, the wavelength of the lasers in many commercial optical tweezers operate in the near infrared to avoid damaging living cells [14 - 16]. An optical trap or "optical tweezer" is a device which can apply and measure piconewton sized forces on micron sized dielectric objects under a microscope using a highly focused light beam. It allows very detailed manipulations and measurements of several interesting systems in the fields of molecular and cell biology and thus acts as a major tool in biophysics [17]. Optical tweezers are used to manipulate biological cells such as human red blood cells [3] to study its elastic properties.

2.2 Laser Trap Fundamentals

The practice of using laser radiation pressure to optically trap small particles has been around for nearly five decades, beginning with Arthur Ashkin at Bell Labs in 1970 [18]. The trapping of micro-sized particles (in our case cells) with size (diameter d) larger than the wavelength of the light, λ, ($d >> \lambda$), can be explained using geometrical optics [19].

Observationally, a dielectric particle in the region of the focused laser beam will be pulled into the high intensity region. This high intensity region is the laser trap. In the absence of the trap, the particle displays Brownian motion. Yet, when the laser is turned on again the particle is again attracted to the region of high intensity and the particle is again trapped. It is apparent that there is a force attracting the particles to the high intensity region of the laser. This attraction to the high intensity region can be understood by examining the forces resulting from the refraction of light.

2.2.1 Force Affecting Trapped Particles

There are two types of forces that affect the trapped particles. Those are the (1) gradient force and (2) scattering force, which exert themselves on a particle and trap particles in the path of the laser beam [20]. The gradient force is a result of the electric field gradient present when a laser beam is focused and photons are aligned. This electric field is strongest at the narrowest part of a focused beam, the beam waist. The dielectric particles to be studied in the

optical trap become attracted to the electric field gradient of the beam waist. The second force affecting dielectric particle movement, the scattering force, is due to the change in momentum experienced by photons traveling in the direction of beam propagation. This force slightly displaces the trapped particle downstream from its original position at the center of the beam waist.

As a result of the combination of both the scattering and gradient force, a particle will be trapped in the optical tweezers apparatus slightly downstream of the laser beam waist [20]. The lateral displacement from the center of the beam is dependent on the strength of the scattering force and the stiffness of the optical trap. The optical trap stiffness can be thought of as the effective spring constant, k, of Hooke's Law [21]. Trapping only occurs when the gradient force is stronger than the scattering force.

2.2.2 Modeling Optical Trapping Forces

Predictions on the affect optical forces have on trapped beads are directly dependent on the diameter of the bead relative to the wavelength of the incident laser. The ray optics model is sufficient to explain how forces trap and displace bead particles only when the radius of the particle is much larger than the wavelength of the trapping laser ($R >> \lambda$) while the radius of the trapped particle is much smaller than the incident light wavelength ($R << \lambda$), then the particle can be treated as an electric dipole and the electric dipole approximation can then be used to predict force interactions.

The Ray Optics Model

When the diameter of the trapped particle is far greater than the wavelength of the incident laser, the classic ray optics model of ray refraction can be used to describe the affect scattering forces have on trapped particles and the resulting gradient forces which withstand the scattering effects and keep the particle trapped just downstream of the beam center. As seen in Figure 2.1, a ray of light entering as "b" is refracted into the sphere and exits at an angle. The change of momentum results in a force in the direction of F_b as

$$\vec{F} = \frac{d\vec{p}}{dt} \tag{2.2.1}$$

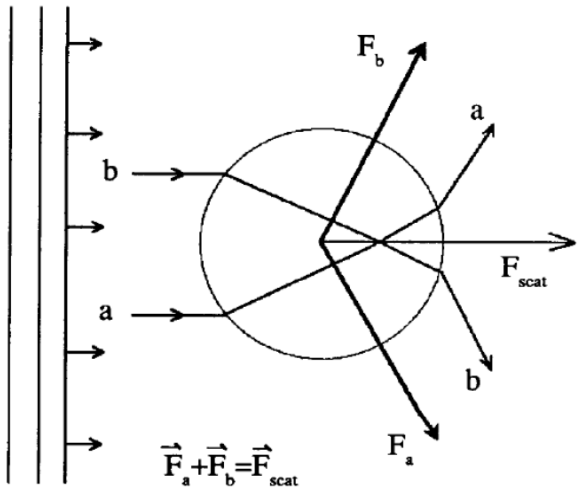

Figure 2.1: Forces on spherical particle centered in a laser trap with particles size greater than the laser wavelength. The resulting scattering force propels them in the direction of the beam [18].

This also occurs for a ray at position "a", which results in a force in the direction of F_a. It can be argued that all the forces due to rays of light would combine to give F_{scat}, as any vertical components would cancel due to symmetry. This is the scattering force, or the force due to the radiant pressure. It is in the direction of the laser beam. It is important to note that due to Snells Law,

$$n_1 \sin\theta_1 = n_2 \sin\theta_2 \tag{2.2.2}$$

the beam will only be refracted internally if the index of refraction of the surrounding fluid is less than that of the particle. If the index of refraction of the surrounding fluid is greater than that of the particle, the particle will be repelled from the point of high intensity [18].

Assuming a Gaussian shaped beam, the maximum intensity exists at the center of the beam. Any particle that is not centered on this maximum intensity is again subject to net force due to the change of momentum of the light rays that are being refracted in the particle. However, unlike before, these forces are not symmetric about the direction of the laser beam. Figure 2.2 shows that how the force due a ray coming from a higher intensity area, such as "a" creates a larger force than that of "b", which would consequently come from a lower intensity area. It can be seen that in addition of the scattering force there is also a gradient force, F_{grad}, due to this imbalance of between rays "a" and "b". This gradient force pulls the particle towards

the point of highest intensity. Whenever the particle is centered on the point of highest intensity, the gradient force disappears as "a" and "b" are once again symmetric. It is this gradient force that traps the particle at the point of greatest intensity of the laser beam [18].

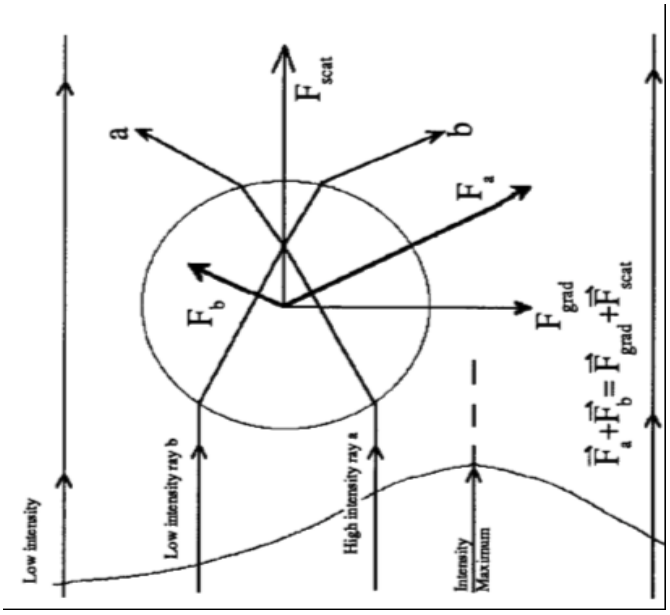

Figure 2.2: Forces on spherical particle centered in a laser trap with particles size greater than the laser wavelength. The resulting scattering force propels them in the direction of the beam and the resulting additional gradient force (exerted on particles not far from the beam axis) draws them towards the region of highest light intensity [18].

The Electric Dipole Model

Once the radius of the particle to be trapped is sufficiently less than the wavelength of the incident laser beams, then the electrical dipole model can be used to approximate the photon and particle interactions. Because the trapped bead is so much smaller than the laser wavelength, it can be thought of as a point dipole in the photon electromagnetic field.

The force acting on a single point charge placed in a magnetic field is called a Lorentz force [22] and can be mathematically described through the equation:

$$\vec{F} = (\vec{p}.\nabla)\vec{E} + \frac{\partial \vec{p}}{\partial t} \times \vec{B} \tag{2.2.3}$$

where $\vec{F}$ is the force, $\vec{E}$ is the electric field, $\vec{B}$ is the magnetic field and $\vec{p} = q\vec{d}$ is the induced dipole moment in the trapped particle.

The trapped particle is linear. We can then eliminate the dipole moment from equation (2.2.1) through the use of the polarizability of the particle to the surrounding medium, α. This porarizability depends on the medium refractive index, n_m and the relative index of the particle to the index of the surrounding medium, n_c, where $\vec{p} = \alpha\vec{E}$. Equation (2.2.1) can be then be rearranged into the form of:

$$\vec{F} = \alpha[(\vec{E}.\nabla)\vec{E} + \frac{\partial\vec{E}}{\partial t} \times \vec{B}] \tag{2.2.4}$$

Using the identity

$$\nabla(\vec{A}.\vec{B}) = \vec{A} \times (\nabla \times \vec{B}) + \vec{B} \times (\nabla \times \vec{A}) + (\vec{A}.\nabla)\vec{B} + (\vec{B}.\nabla)\vec{A}$$

$$(\vec{E}.\nabla)\vec{E} = \frac{1}{2}\nabla E^2 - \vec{E} \times (\nabla \times \vec{E}) \tag{2.2.5}$$

$$\frac{\partial\vec{E}}{\partial t} \times \vec{B} = \frac{\partial}{\partial t}(\vec{E} \times \vec{B}) - \vec{E} \times \frac{\partial\vec{B}}{\partial t} \tag{2.2.6}$$

And using Maxwell's equation,

$$\nabla \times \vec{E} = -\frac{\partial}{\partial t}\vec{B}$$

Eq.(2.2.6) can be written as

$$\frac{\partial\vec{E}}{\partial t} \times \vec{B} = \frac{\partial}{\partial t}(\vec{E} \times \vec{B}) + \vec{E} \times (\nabla \times \vec{E}) \tag{2.2.7}$$

Upon substititing Eq.(2.2.5) and Eq.(2.2.7) into Eq.(2.2.4) we obtain

$$\vec{F} = \alpha[\frac{1}{2}\nabla E^2 + \frac{\partial}{\partial t}(\vec{E} \times \vec{B})] \tag{2.2.8}$$

The last term on the right-hand side of equation (2.2.8) is the time derivative of the Poynting vector, which represents the power flux through an electromagnetic field. During the optical tweezers experiment, the sampling frequencies are much shorter than the frequency of the laser beam, $\sim 10^{14}$ Hz, and so the power of the laser will be constant [13]. Constant power will lead to a zero value of the time derivative of the Poynting vector and so this term can be removed from the equation. The force acting on the electric dipole can then be represented with the equation:

$$\vec{F} = \alpha\frac{1}{2}\nabla E^2 \tag{2.2.9}$$

Because the E^2 term in equation (2.2.9) represents the electromagnetic intensity of the photons, the strongest light forces acting on the particle will be those with the highest intensity. As the peak photon intensity occurs at the center of the beam waist, the forces acting on the bead to be studied will draw it to this position. These forces are then of gradient type, as they attract particles to the center of the beam.

Chapter 3

Experimental Methods

As it was discussed in the introduction, this work is primarily focused on analysis of the data collected at biomedical optics lab at MTSU. However, we have studied several visual records that describe how the measurements conducted in this lab to collect such data that is analyzed in this work. This chapter will discuss the experimental methods use to produced the data studied.

3.1 Hemoglobin Quantitation and Sample preparation

First the four blood samples were diluted in fetal bovine serum in about a 1:1000 ratio. Each of these samples was placed in a well slide for trap measurements. Four blood samples drawn from four individuals in one family were studied in this work. This family consists of the two parents and their two twin babies. The hemoglobin quantitation of these unidentified individuals blood sample was carried out at the sickle cell center at Meharry Medical Collage in Nashville, Tennessee, USA. Hemoglobin types and relative percentages were assessed by HPLC for each of the four blood samples and the result is given in Table 3.1.

Hb quantitation for the male parent is Hb AS with 42.8% HbS and 52.3% HbA and the female parent is Hb AC with 41.09% HbC and 55.4% HbA. Since nearly half of the Hb in both parents are abnormal genetically mutated genes (S and C), these parents carry a SCT. The Hb quantitation for their infant baby girl is Hb FA with 70.1% HbF and 29.1% HbA and baby boy is Hb FSC with 82.6% HbA, 7.1% HbS and 7.1% HbC

Blood sample	Hb AS	Hb AC	Hb FSC	Hb FA
Sex	M	F	M	F
Age	38 years	30 years	75 days	82 days
Draw Date	2016/2/17	2016/2/17	2016/2/2	2016/2/17
Delivery Date	2016/2/18	2016/2/18	2016/2/4	2016/2/18
HPLC measurement date (Y/M/D)	2016/2/18	2016/2/17	2016/2/5	2016/2/18
Laser trapping date (Y/M/D)	2016/2/21	2016/2/25	2016/2/20	2016/2/20
Relative percentage of each hemoglobin type				
Hb A(%)	53.20	55.41	0.00	29.10
Hb A_2(%)	3.60	3.10	0.20	0.80
Hb C(%)	0.00	41.09	7.10	0.00
Hb F(%)	0.40	0.40	82.60	70.10
Hb S(%)	42.80	0.00	7.10	0.00
Basic statistical parameters describing the of distribution				
Average diameter (μm)	7.93	7.86	6.51	6.47
Standard deviation	0.64	1.07	0.81	0.66

Table 3.1: Relative percentage of hemoglobin types by HPLC and RBCs size measurements by Image-Pro Plus 6.2 programming software.

Such Hb quantitation for the infants indicate that the baby girl is normal but the baby boy has two abnormal genetically mutated genes (S and C), the baby boy carry a SCA.

3.2 Laser Trapping

The design for the complete set-up of the experiment is shown Fig.3.1. The main elements of this experimental set-up are a high power infrared diode laser (8 watts at 1064 nm), an inverted microscope equipped with a high numerical aperture, and a computer-controlled digital camera. The laser was a linearly polarized infrared diode laser source (LS) with a maximum power of 8 watts. The original beam size was 4 mm: this was expanded using a 20 $\times$ beam expander (BE). The beam was then again resized to approximately 2 cm using a pair of two lenses (L1 and L2), with focal lengths of 20 cm and 5 cm. Four optical mirrors (M1-4) were used to direct the beam into the dichroic mirror (DM) at the laser port of the inverted microscope (IX 71-Olympus). The dichroic mirror is angled at 45° such that the reflected light makes an angle normal to the incident light. The aligned beam would then be reflected into the back of the objective lens (OL) that has a 100 $\times$ magnification and a 1.25 numerical aperture. Two lenses (L3 and L4) are

positioned such that the laser trap is on the focal plane of the microscope. The microscope is equipped with a computer controlled piezo-driven stage (PS) and a digital camera (DC) used to take a live 2D bright-field contrast image of the sample by a 30 mW halogen lamp (HL). Both the piezo-driven stage and the digital camera are interfaced with a computer (PC). The power of the laser was controlled by a $\lambda/2$-wave plate (W) and a polarizer (P). At the location of the trap

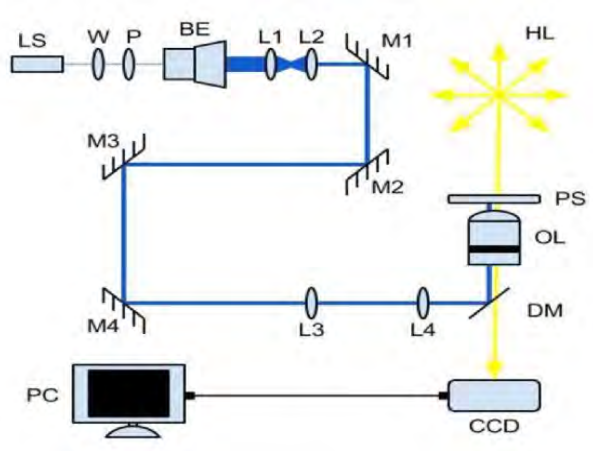

Figure 3.1: Laser trap experimental set up: laser source (LS), $\lambda/2$-wave plate (W), polarizer (P), dichroic mirror (DM), optical lens (OL), and digital camera (CCD) [4].

there was 15% efficiency with respect to the power measured before the fourth lens, L4. The power before L4 was measured near the focal point of L3 using a high-power meter calibrated at 1064 nm wavelength. We then measured power at the trap location, using the same power meter placed on top of the microscope stage with head covering the tip of the objective lens. This efficiency was used to keep the power the same at the trap location where for each cell was trapped and ionized in this study.

The samples prepared in well-slide is then placed on the microscope stage then the gate for the laser port is opened. Each RBCs of the four blood samples observed while it was being trapped, ionized, and ejected from the trap when the laser is turned on. At this instant the digital camera is turned on and captured consecutive images at a rate of 0.12 second per frame. Selected frames for the four samples of RBCs describing this process are shown in Fig.3.2. The line colored red in Fig. 3.2. connects positions of the RBC from selected images captured when the RBCs as it accelerating towards the trap. This part of the trajectory was observed for when the RBCs positioned off the center of the trap. When an RBC is positioned in line with the

center of the trap, the cell will instantly shrunken and trapped and the cell becomes ionized (charged) and begin to get ejected as shown by the two images connected by the green horizontal line in Fig. 3.2 the cell was staid at the trap until the cell was fully charged. Due to the charge developed on the cell, it experienced an electrostatic force due to the electric field of the laser beam. After the cell was fully charged, the electrostatic force due to the electric field of the laser beam is greater than the gradient force (trapping force), the cell was forced to be ejected from the trap and the post ionization trajectory of the RBC is shown by the blue line traced along its positions at different times selected from the images captured while the cell is moving away from the trap.

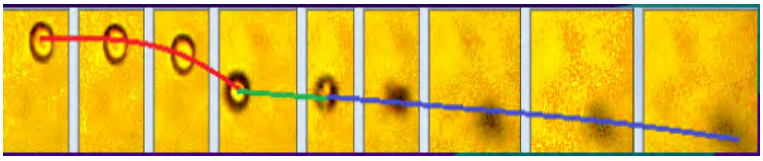

Figure 3.2: The snap shots describing the trajectories of a RBC as it moves towards the trap (red) and as it recedes from the trap after it is charged and ejected from the trap (blue).

We have carried out this procedure for a total of 62 cells for Hb AS, Hb FSC, and Hb FA and 47 cells for Hb AC .

Chapter 4

Data Analysis and Results

In this chapter we have determined the average volume and the average mass of the four blood samples using the respective measured average diameter of blood sample cells and the widely accepted density of red blood cells. In addition to this we have determined the average amplitude of the electric field (E_0) of the laser beam at the trap location using the power of the laser at the trap location, the velocity of light in the medium that the cells are suspended in and the laser beam area (A), which is determined from the beam size. And also we have discussed in detail about the theoretical model that we develop to determine the charge developed during ionization and the stiffness (the trapping force constant). The model is based on the trajectory of the cell after it eject from the trap.

4.1 Preemptive Analysis

Using the software Image Pro, a conversion factor was found for pixels to meters by measuring silicon beads that had a known diameter. This value was 7.27×10^{-8} meters per pixel. Using the captured images of the cells before they were trapped, the diameter of the cell was measured. A spherical cell was assumed to determine the volume of each cell. The mass of each cell was found for four different blood samples by using the widely accepted density of red blood cells of 1098.8 kg/m^3 [23]. Using the average volume $2.66 \times 10^{-16} m^3$ calculated using the measured average diameter of the cells, the average mass of the cells was found to be 2.92×10^{-13} kg for AS hemoglobin type, using the average volume $2.55 \times 10^{-16} m^3$ calculated using the measured average diameter the cells, the average mass of the cells was found to be 2.80×10^{-13} kg for AC hemoglobin type, using the average volume $1.51 \times 10^{-16} m^3$ calculated using the measured average diameter of the cells, the average mass of the cells was found to be 1.66×10^{-13} kg

for FSC hemoglobin type and using the average volume $1.46 \times 10^{-16} m^3$ calculated using the measured average diameter of the cells, the average mass of the cells was found to be 1.60×10^{-13} kg for FA hemoglobin type.

To find the average amplitude of the electric field, E_0, the Poynting vector of the laser beam was used in conjunction with the recorded power, P, at the trap location [25]

$$\vec{S} = \frac{1}{\mu_0} \vec{E} \times \vec{B} \tag{4.1.1}$$

Thus for the power, P, laser beam area, A, and accounting for the time averaging of the sinusoidal electric field

$$S = \frac{P}{A} = \frac{EB}{\mu_0} = \frac{{E_0}^2}{2v\mu_0}$$

The amplitude of the electric field at the trap location can be evaluated by [25]

$$E_0 = \sqrt{\frac{2Pv\mu_0}{A}} \tag{4.1.2}$$

where v is the speed of light in the medium that the cells are suspended in. The power of the trap used was recorded at the location of the trap for each cell. On average the power at the trapping location was 355.80 mW, 374.55 mW, 361.50 mW and 358.95 mW for Hb AS, Hb AC, Hb FSC and Hb FA respectively. For v we used the speed of light in water, $v = 2.25 \times 10^8$m/s and vacuum permeability, $\mu_0 = 4\pi \times 10^{-7} Hm^{-1}$. The beam size is estimated, following the method by Lian *et al.* [24], using $w = (d_0 \cos(2\alpha_{max}) + z_0) \tan(\alpha_{max})$, that depends on the size of the cell (d_0), position of the trap (z_0) as measured from the tip of the objective lens, and the maximum angular position of the incident ray with respect to the beam axis (α_{max}). α_{max} is determined by the numerical aperture (NA) of the objective lens and the refractive index of the surrounding medium (n_{water}), such that $NA = n_{water} \sin(\alpha_{max})$. For our trap, $NA = 1.25$ and $n_{water} = 1.33$ which gives $\alpha_{max} = 78°$. Thus with $d_0 = 7.93\mu m$, $d_0 = 7.86\mu m$, $d_0 = 6.51\mu m$, and $d_0 = 6.47\mu m$ and $z_0 = 100\mu m$ (the thickness of the cover-slip), the beam size is estimated to be $436.38\mu m$, $436.68\mu m$, $442.49\mu m$, and $442.67\mu m$ for AC, AS, FSC, and FA hemoglobin type respectively.

4.2 Theoretical Model

4.2.1 Newtonian Mechanics

Due to the electric field of the laser, the cell was subject to an electrostatic force because of the charge developed due to dielectric breakdown.

$$\vec{F_E} = q\vec{E} \tag{4.2.1}$$

Where as q is the total charge of the cell and E is the electric field of the laser. During the course of the dielectric breakdown, the cell was building up a greater and greater charge, such that q is a function of time. Consequently, the electrostatic force on the cell is growing stronger and stronger. When the electrostatic force is greater than the intensity gradient trapping force of the laser trap, the cell will be pushed out or ejected from the laser trap. At this point the charge on the cell is constant.

For the theoretical model, we consider three forces acting on the cell with mass m ejected from the trap at a distance r from the center of the trap, at a given time t. These forces were the electrostatic force, F_E, the drag force, F_D, and trapping force of the laser which is related to the gradient of the electric field, F_T. The electrical force and the trap force depend on the electric field strength at the position of the cell r measured from the center of the trap. Since the laser beam is Gaussian, which is a beam of electromagnetic radiation whose transverse electric field distribution is described by Gaussian function. Thus the Gaussian beam of the electric field amplitude at distance r is given by

$$E(r) = E_0 \exp(-\frac{r^2}{\omega_0^2}) \tag{4.2.2}$$

As we know, a charge, q, moving with the velocity, $\vec{v}$, in an electromagnetic field, containing both an electric, $\vec{E}$, and magnetic, $\vec{B}$, fields, experiences a force

$$\vec{F} = \vec{F_E} + \vec{F_M} = q(\vec{E} + \vec{v} \times \vec{B}) \tag{4.2.3}$$

Where $\vec{F_E}$ is the electrical force due to electric field and $\vec{F_M}$ is the magnetic force due to magnetic field.

The electromagnetic force that depend on the charge developed on the ejected cell is directly proportional to the electric field only. Because of the velocity of the moving charge parallel to the magnetic field ($\vec{v} \times \vec{B} = 0$) . Using Eq.(4.2.2) which is written as

$$F_E = qE_0 \exp(-\frac{r^2}{\omega_0^2}) \tag{4.2.4}$$

The drag force due to the viscosity of the medium is equivalent to

$$F_D = -\beta \frac{dr}{dt} \tag{4.2.5}$$

Where Stokes law was used to describe the drag coefficient, such that $\beta = 6\pi\mu R$, as the cells were assumed to be spherical with radius R in a fluid with viscosity μ. The viscosity of the growth media RPMI-1640 was approximated to be on the same order of water, which at room temperature is $1.0 \times 10^{-3} Ns/m^2$.

The trapping force is proportional to the gradient of the electric field in Eq. (4.2.2) squared and it can be found using the Lorentz force, assuming an electric dipole approximation for the cell.

$$F_T = \frac{1}{2}\alpha\nabla(E(r))^2 = \frac{1}{2}\alpha\nabla(E_0 \exp(-\frac{r^2}{\omega_0^2}))^2 \tag{4.2.6}$$

Using Newton's second law, the net forces acting on the cell just after it ejected from the trap can be written as

$$m\vec{a} = \vec{F_E} + \vec{F_D} + \vec{F_T} \tag{4.2.7}$$

Upon substituting Eq.(4.2.4), Eq.(4.2.5), and Eq.(4.2.6) into Eq.(4.2.7), we obtain

$$m\frac{d^2r(t)}{dt^2} = qE_0 \exp(-\frac{r^2(t)}{\omega_0^2}) - \beta\frac{dr(t)}{dt} + \frac{1}{2}\alpha\nabla(E_0 \exp(-\frac{r^2(t)}{\omega_0^2}))^2 \tag{4.2.8}$$

Where α is a constant that depends on the relative dielectric susceptibility of the ionized cell with respect to the medium, the refractive index of the surrounding, the refractive index of the cell and also its size. It is important to note that the electrical susceptibility that the cell has during the post ionization period should be significantly lower than its natural electrical susceptibility. This should be expected because while the cell was in the trap, it was undergoing dielectric breakdown and continually developed charge due to the incident radiation from the trap.

In order to solve the differential equation in Eq.(4.2.8), we had to make physically reasonable approximation. We assumed the electrical force does not vary significantly over the range of the distance r in which we measured and analyzed. We can write Eq.(4.2.4) as

$$F_E = qE_0 \tag{4.2.9}$$

Similarly, over this range of distance, the trapping force is approximated like a spring force. The approximation for the trapping force was made by making a series expansion for the electric field and keeping terms up to the first in r. We can write Eq.(4.2.6) as

$$F_T = -kr(t) \tag{4.2.10}$$

Upon substituting Eq.(4.2.9) and Eq.(4.2.10) into Eq.(4.2.8), we obtain

$$\begin{aligned} m\frac{d^2r(t)}{dt^2} &= qE_0 - \beta\frac{dr(t)}{dt} - kr(t) \\ \implies m\frac{d^2r(t)}{dt^2} + \beta\frac{dr(t)}{dt} + kr(t) &= qE_0 \end{aligned} \tag{4.2.11}$$

The right hand side of Eq.(4.2.11) represents the electrostatic force due to the charge, q, developed on cell due to the ionization by the radiation at the instant it got ejected from the trap. The second term represents the damping force due to the viscosity of the fluid in which the cell is suspended. The third term represents the trapping force that constantly keeps trying to suck the cell back to the center of the trap. The constant k is the trapping force constant that depends on the magnitude of the induced polarization in the ionized ejected cell. It also depends on the dielectric susceptibility of the ionized cell and the amplitude of the electric field of the trap. This constant varies from one cell to another. It is important to note that even though each cell carries a net charge due to the ionization by the radiation while it was trapped, it also has a smaller induced electrical polarization as it recedes away from the center of the trap. This induced polarization is primarily due the electric field of the laser trap, which could be amplified or diminished by the net charge developed on each cell. It could also vary from one cell to another depending on the size of the cells.

Equation (4.2.11) is an equation for a damped harmonic oscillator of mass m and charge q driven by a uniform electric field E_0. Using initial conditions just before the cell is ejected from the

trap, it is considered to be at rest at the center of the trap. The solution was found to be [25]

$$r(t) = \frac{E_0 q}{k}[1 - \exp(-\frac{\beta t}{2m})[\cosh(\frac{\sqrt{\beta^2 - 4km}}{2m}t) + \frac{\beta}{\sqrt{\beta^2 - 4km}}\sinh(\frac{\sqrt{\beta^2 - 4km}}{2m}t)]] \quad (4.2.12)$$

This is an equation governing the displacement of the cells as measured from the center of the laser trap based on the forces acting upon them. The numerical model fitting function NonlinearModelFit in Mathematica was used to fit this model of displacement versus time data for each cell, where the mass, m, drag coefficient, β, and electric field, E_0, are known for each cell. Equation (4.2.11) is an equation of an electrically driven damped harmonic oscillator. Our experimental data indicated that each cell, after being driven out of the trap, quickly loses its momentum as it recedes away from the center of the trap. Thus the motion of the cell must be an over damped electrically driven harmonic oscillator. This requires the solution in Eq. (4.2.12) must remain hyperbolic and should not become trigonometric. A trigonometric solution would predict under damped oscillatory motion for the cells that is contrary to the evidence provided by our experimental data. Consequently, we must choose $\beta^2 \geqslant 4km$. Physically, this means that after the cell is ionized and ejected from the trap, the force due to the induced polarization of the cell that was constantly trying to suck cell back to the trap must be smaller than the drag force. This could certainly prove that, while the cell was in the trap, it had gone through an irreparable dielectric breakdown due to the high dose of radiation it absorbed that most likely lead to its death [25].

The maximum value of k for each cell was found by solving for k from $\beta^2 - 4km = 0$ using the average mass and drag coefficient of each cell. Using the NonlinearModelFit function started looking for k at several orders of magnitude below the maximum value. Which is shown in the table below.

Blood sample	Hb AS	Hb AC	Hb FSC	Hb FA
Sex	M	F	M	F
Age	38 years	30 years	75 days	82 days
maximum value of k (N/m)	0.005	0.005	0.0097	0.0095
Standard deviation	0.00067	0.0004	0.004	0.003
Average value of k (N/m)	3.17×10^{-7}	3.19×10^{-7}	3.42×10^{-7}	2.91×10^{-7}
Standard deviation	1.05×10^{-7}	1.05×10^{-7}	1.11×10^{-7}	9.03×10^{-8}

Table 4.1: The statistical analysis of trapping coefficient (trapping stiffness) for the four RBCs samples.

There were slight variances in the trapping coefficient k for each cell. As previously stated, k is proportional to the cells polarization that is significantly diminished by the damage due to the absorbed radiation while the cell was in the trap. This weak remnant polarization also depends on the cell size and the polarizing electric field. The effect of the electric field diminishes as the cells receding from the center of the trap due to the Gaussian nature and the reduced beam waist of the laser beam by the microscope objective lens.

Chapter 5

Results and Conclusion

5.1 Experimental Results

The study of our experimental results are presented and discussed in this section. We will focus on the individual and average relevant physical properties during ionization and after the cell eject from the trap for the 62 RBCs for AS, FA, and FCS and 47 RBCs for AC studied from in the blood sample.

The results of the experiment are depicted in Fig. 5.1, which shows the displacement of the four blood samples cell from the center of the laser trap as a function of time.

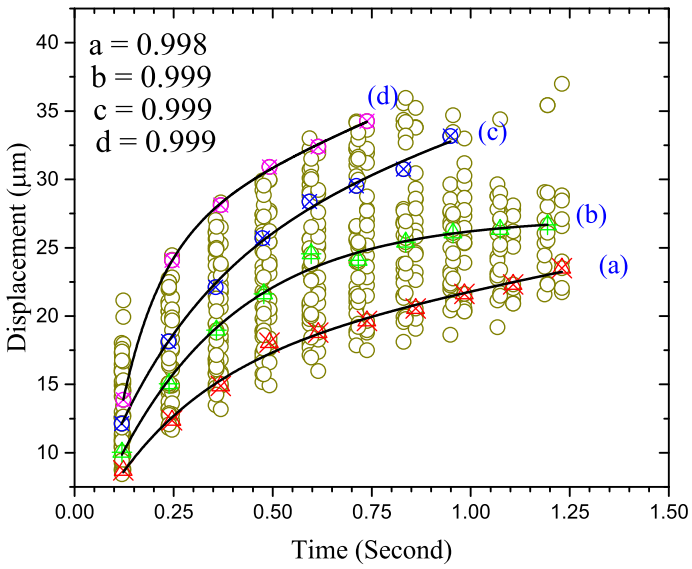

I.Displacement for all ejected 62 Hb AS cells as measured from the center of the trap as a function of time.

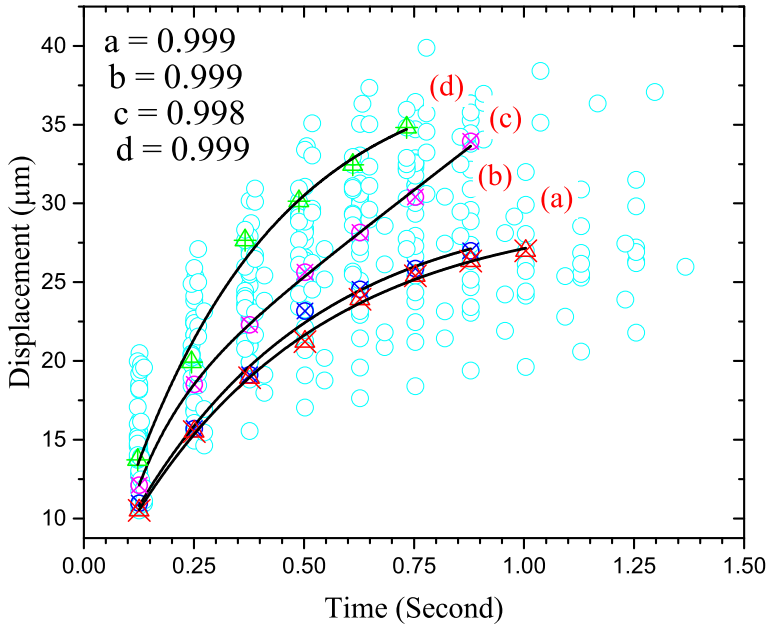

II.Displacement for all ejected 47 Hb AC cells as measured from the center of the trap as a function of time.

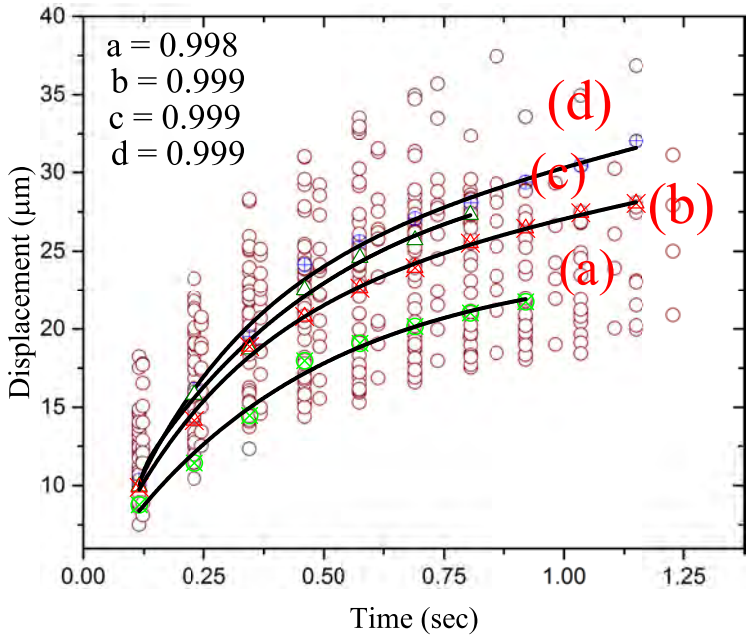

III.Displacement for all ejected 62 Hb FSC cells as measured from the center of the trap as a function of time.

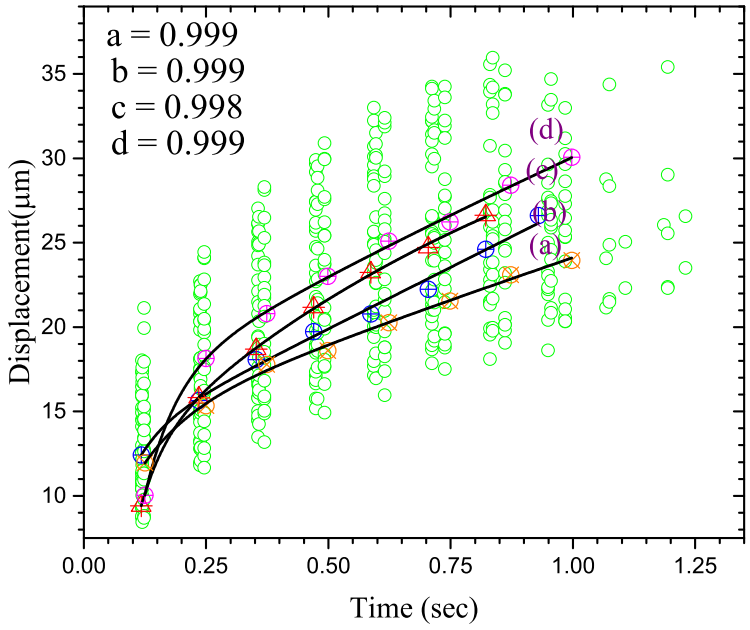

IV.Displacement for all ejected 62 Hb FA cells as measured from the center of the trap as a function of time.

Figure 5.1: The displacement of the four blood samples ejected cells as measured from the center of the trap as a function of time.

The function found the unknown constants of the charge on the cell, q, and the trapping coefficient, k, within a confidence interval of 0.99. The determination of agreeance values, R^2, are extremely high for all cells of the four blood samples, with the lowest value being 0.992, 0.995, 0.992. 0.993 for Hb AS, Hb AC, Hb FSC and Hb FA respectively. The mean R^2 values are 0.997 for four blood samples. Thus, theoretical model had extremely high agreeance with the experimental data.

For illustration purpose, the fitting of the solution described by Eq. (4.2.12) (described by the block solid lines) to the experimental data (symblols colored) for four cells of the four blood samples are displayed in Fig. 5.1 (I - IV). The curves fitted to the experimental data of these four cells of the four blood samples had R^2 values of: a = 0.998, b = 0.999, c = 0.999, and d = 0.999 for Hb AS, a = 0.999, b = 0.999, c = 0.998, and d = 0.999 for Hb AC, a = 0.998, b = 0.999, c = 0.999, and d = 0.999 for Hb FSC and a = 0.999, b = 0.999, c = 0.998, and d = 0.999 for Hb FA which indeed shows extremely high agreeance values.

The threshold ionization energy (TIE), the threshold radiation dose (TRD), and the relation of TIE and also TRD to the sizes of the cells were studied. The TIE is the minimum energy incident on the cell during the instant the it got trapped to the instant it got ejected. It was determined from the measured incident power at the trap location ($P_T = P * 0.15$), where P is the power of the laser, which was the same for all cells of the given sample but different for the four blood samples and using the ionization period for each cells (T_C), $TIE = P_T * T_C$). Commonly, the TRD required to ionize and kill a cell is measured by the amount of energy absorbed by the cell per unit mass. The mass is proportional to the volume which depends on the diameters of the RBCs, if we use the closest spherical model for a RBC. Since the accurate thickness of each cells can not be determined from the two-dimensional images captured, the TRD were studied in using the area (A_C) instead of mass (m_C). Thus, the TRD were calculated using the TRD = TIE/A_C in units of $mJ/\mu m^2$ for each cells. The relation of the TIE and TRD to the size of the cell were also studied using the measured diameter of the cells prior to trapping.

The results for the diameter, the TIE, and TRD for all four blood samples RBCs studied are displayed using color coded double axes histogram in Fig. 5.2 - 5.5 of (a). In Fig 5.2 - 5.5 of (a), both the right and left vertical axes represent the number of cells but in the horizontal axes, while the top axis (colored green) represent the diameters, the bottom axis represent both the TIE (labeled in blue) and the TRD (labeled in red). The basic statistical parameters to the histograms for diameter (green), TIE (blue), and TRD (red) are shown in Fig. 5.2 - 5.5 of (a) along with the Hb quantitation of four blood samples. The value of the basic statistical parameters such as diameter of the RBCs, TIE and TRD are shown in table 5.1. The TIE and the TRD as a function of the diameter for all four blood samples RBCs are displayed in Fig. 5.2 - 5.5 of (b) using double vertical axes following the same colour codding (TRD in red and TIE in blue). The reduced data for threshold ionization energy (blue), and the threshold radiation dose (threshold ionization energy per unit area) (red) for the four blood samples RBCs are displayed in Fig. 5.2 - 5.5 of (c).

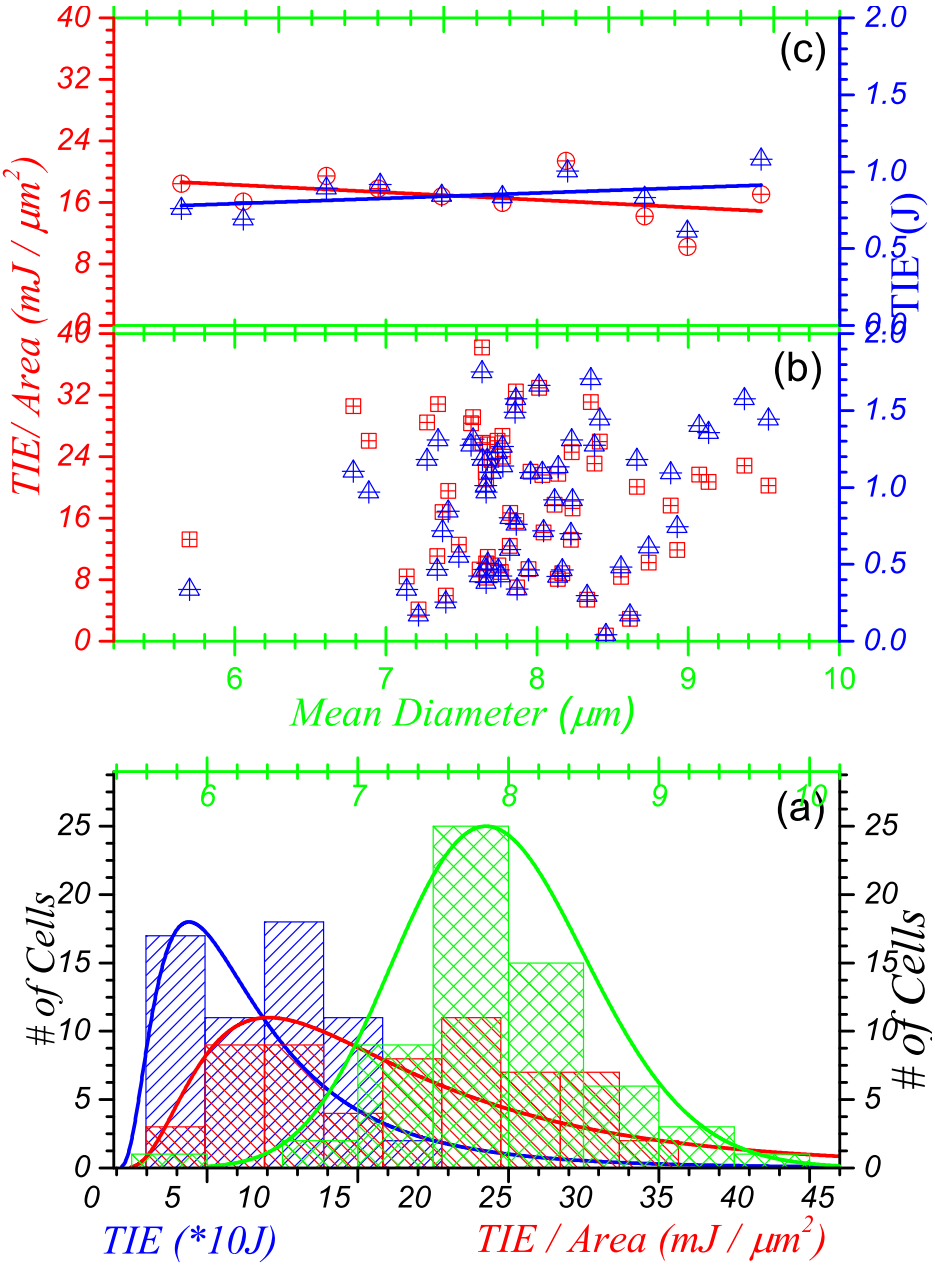

Figure 5.2: The size distribution of the graph shows that statistical distribution of the TIE, TRD, and the measured mean diameter of the RBCs as : (a) the statistical distribution of the mean diameter of the Hb AS blood sample (green), the threshold ionization energy of the Hb AS blood sample (blue), and the threshold radiation dose of the Hb AS blood sample (red), (b) the statistical distribution shows that the threshold ionization energy of the Hb AS blood sample (blue), and the threshold radiation dose of the Hb AS blood sample (red) as a function of the measure mean diameter for a total of 62 cells, and (c) the statistical distribution shows that the reduced data for threshold ionization energy of the Hb AS blood sample (blue), and the threshold radiation dose (the threshold ionization energy per unit area) of the Hb AS blood sample (red) as a function of the measure mean diameter for a total 50 cells.

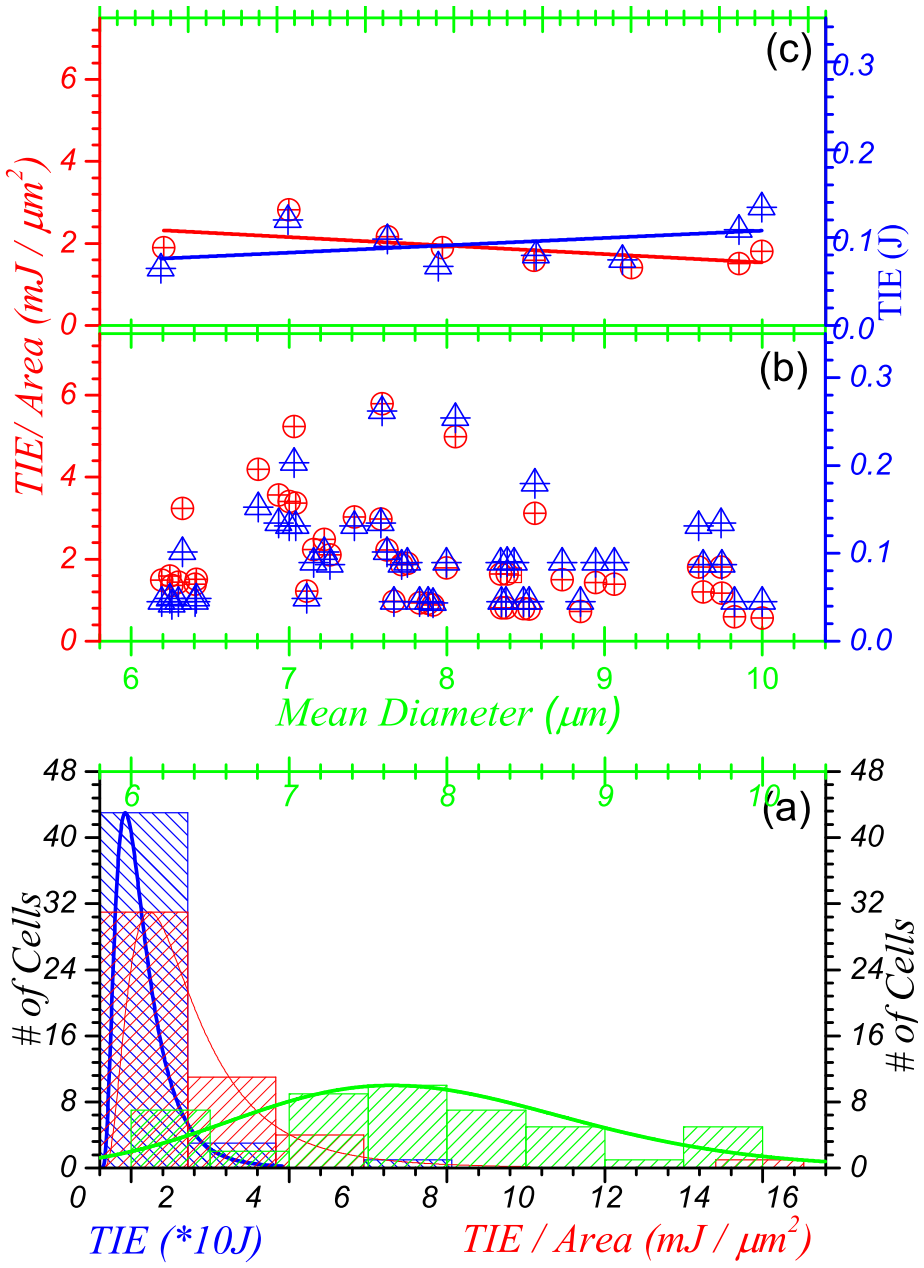

Figure 5.3: The size distribution of the graph shows that statistical distribution of the TIE, TRD, and the measured mean diameter of the RBCs as : (a) the statistical distribution of the mean diameter of the Hb AC blood sample (green), the threshold ionization energy of the Hb AC blood sample (blue), and the threshold radiation dose of the Hb AC blood sample (red), (b) the statistical distribution shows that the threshold ionization energy of the Hb AC blood sample (blue), and the threshold radiation dose of the Hb AC blood sample (red) as a function of the measure mean diameter for a total of 47 cells, and (c) the statistical distribution shows that the reduced data for threshold ionization energy of the Hb AC blood sample (blue), and the threshold radiation dose (the threshold ionization energy per unit area) of the Hb AC blood sample (red) as a function of the measure mean diameter for a total 35 cells.

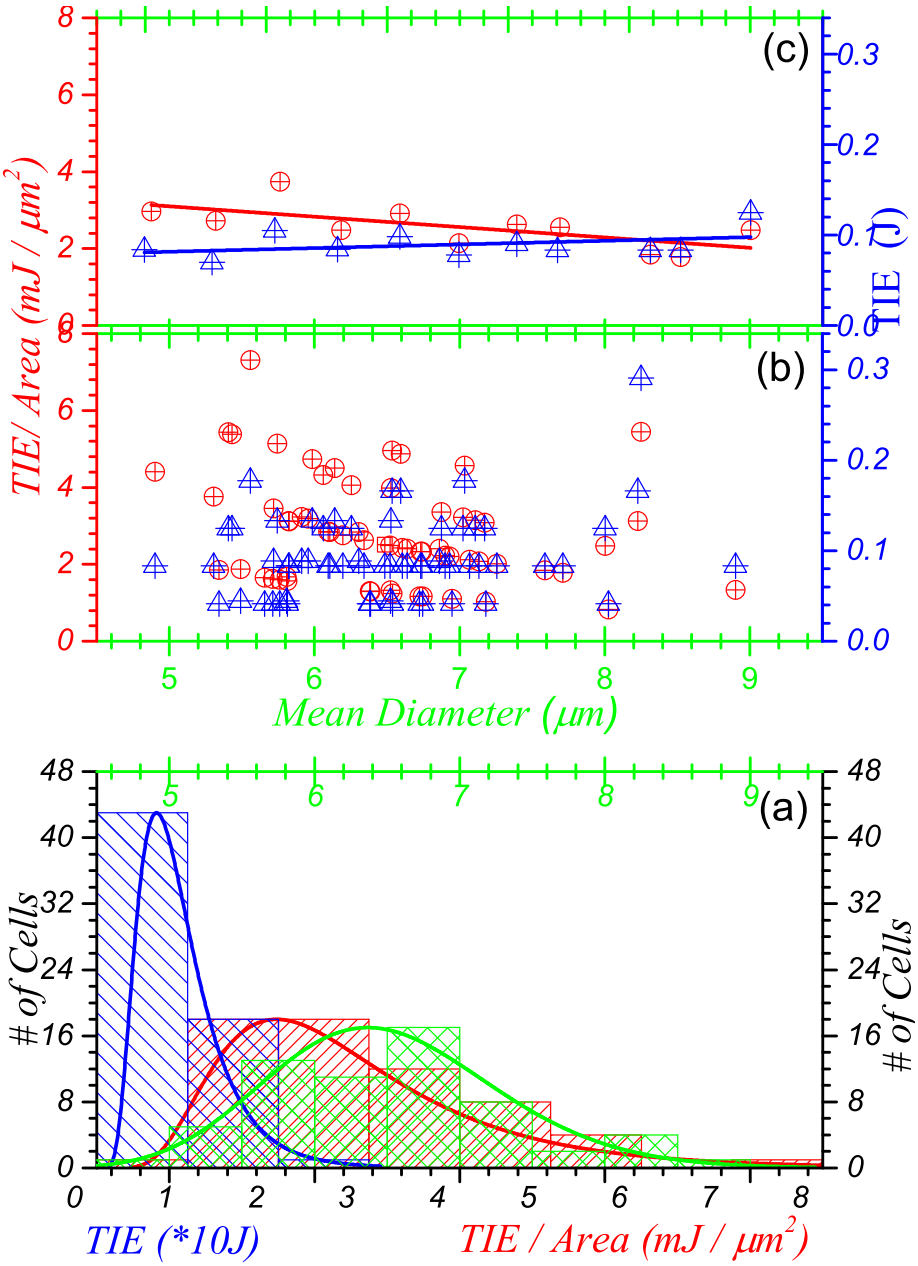

Figure 5.4: The size distribution of the graph shows that statistical distribution of the TIE, TRD, and the measured mean diameter of the RBCs as : (a) the statistical distribution of the mean diameter of the Hb FSC blood sample (green), the threshold ionization energy of the Hb FSC blood sample (blue), and the threshold radiation dose of the Hb FSC blood sample (red), (b) the statistical distribution shows that the threshold ionization energy of the Hb FSC blood sample (blue), and the threshold radiation dose of the Hb FSC blood sample (red) as a function of the measure mean diameter for a total of 62 cells, and (c) the statistical distribution shows that the reduced data for threshold ionization energy of the Hb FSC blood sample (blue), and the threshold radiation dose (the threshold ionization energy per unit area) of the Hb FSC blood sample (red) as a function of the measure mean diameter for a total 52 cells.

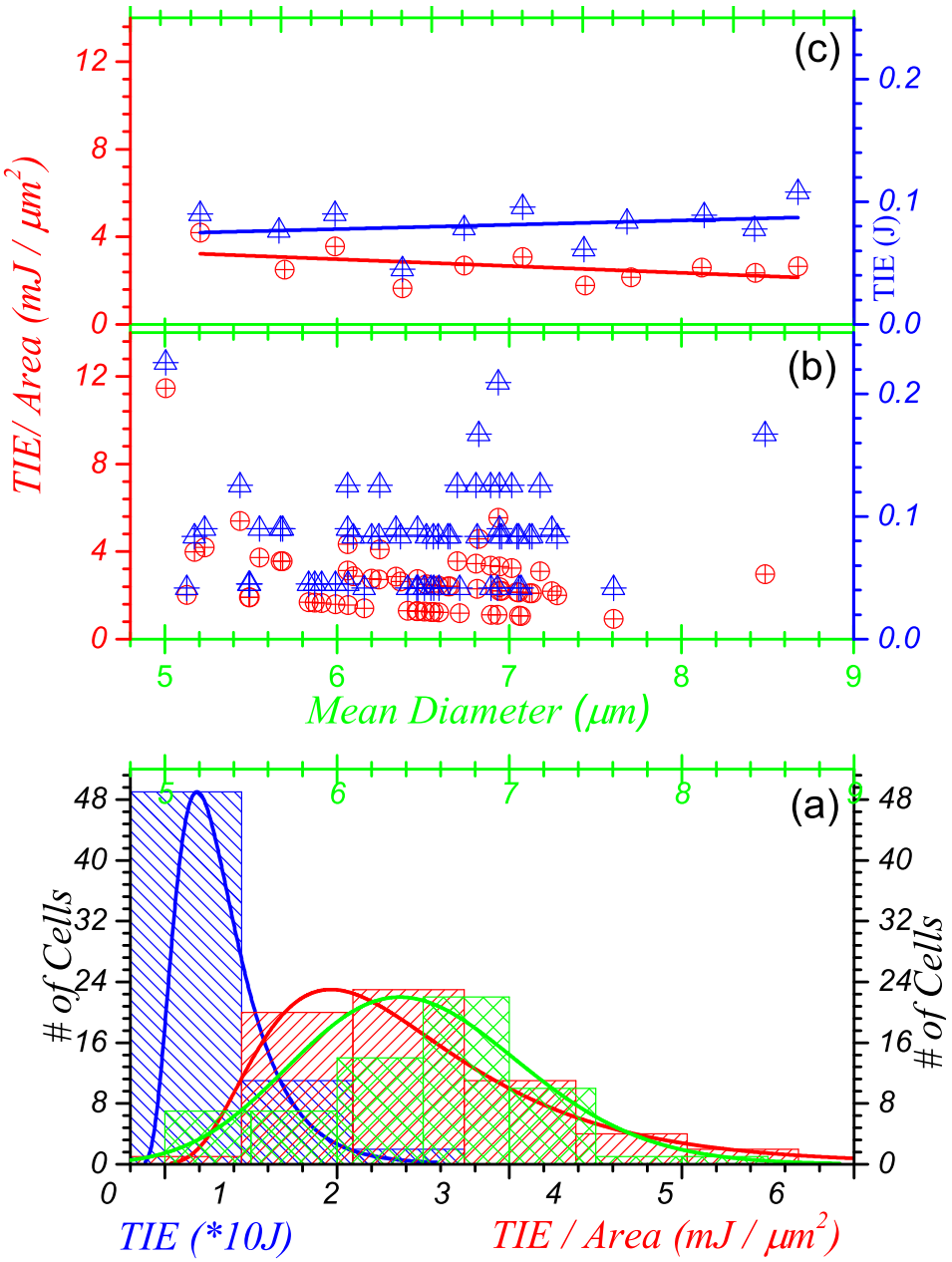

Figure 5.5: The size distribution of the graph shows that statistical distribution of the TIE, TRD, and the measured mean diameter of the RBCs as : (a) the statistical distribution of the mean diameter of the Hb FA blood sample (green), the threshold ionization energy of the Hb FA blood sample (blue), and the threshold radiation dose of the Hb FA blood sample (red), (b) the statistical distribution shows that the threshold ionization energy of the Hb FA blood sample (blue), and the threshold radiation dose of the Hb FA blood sample (red) as a function of the measure mean diameter for a total of 62 cells, and (c) the statistical distribution shows that the reduced data for threshold ionization energy of the Hb FA blood sample (blue), and the threshold radiation dose (the threshold ionization energy per unit area) of the Hb FA blood sample (red) as a function of the measure mean diameter for a total 52 cells.

For detialed information about the statistical parameters for the four blood samples shown in table 5.1 below.

Basic statistical parameters describing the size distribution						
Blood Sample	No of cells	Quantities	Minimum	Maximum	Mean	Std.Dev
Hb AS	62	Diameter (μm)	5.70	9.53	7.93	0.64
		TIE (mJ)	42.48	1750.54	896.97	446.31
		TRD (mJ/μm^2)	0.76	38.22	18.14	8.85
		Charge (nC)	2.18×10^{-7}	8.70×10^{-7}	4.72×10^{-7}	1.59×10^{-7}
Hb AC	47	Diameter (μm)	6.19	10.00	7.86	1.07
		TIE (mJ)	41.77	627.67	103.89	94.46
		TRD (mJ/μm^2)	0.57	15.31	2.27	3.31
		Charge (nC)	2.65×10^{-7}	9.75×10^{-7}	5.34×10^{-7}	1.76×10^{-7}
Hb FSC	62	Diameter (μm)	4.90	8.90	6.51	0.81
		TIE (mJ)	41.57	291.01	92.69	45.96
		TRD (mJ/μm^2)	0.82	7.31	2.84	1.38
		Charge (nC)	2.14×10^{-7}	9.03×10^{-7}	4.81×10^{-7}	1.40×10^{-7}
Hb FA	62	Diameter (μm)	5.00	8.49	6.47	0.66
		TIE (mJ)	41.84	225.40	83.22	41.02
		TRD (mJ/μm^2)	0.92	11.46	2.61	1.58
		Charge (nC)	1.97×10^{-7}	7.34×10^{-7}	3.94×10^{-7}	1.26×10^{-7}

Table 5.1: The values for the basic statistical parameters for the diameter, TIE, TRD, and Charge for four RBCs samples.

As previously mentioned, the NonlinearModelFit function was used to find the unknown constants of the trapping coefficient and the charge developed on each cell. Fig. 5.6 - 5.9 of (a) is a histogram of the amount of charge developed on each of the 62 ionized cells for Hb AS, Hb FSC and Hb FA, and 47 ionized cells foe Hb AC. It is customary to express the magnitude of charge in ionized microscopic compounds or charged molecules, such as Hb, in units of the magnitude of the charge of an electron (e = 1.602×10^{-19} C) known as the Z number [26]. Following this approach, the charge is expressed in units of e (the Z number) in the figure below. The distribution of the charge in Fig. 5.6 - 5.9 of (a) shows that the charge developed varies from 2.18×10^{-16} C to 8.70×10^{-16} C with an average of $4.72 \pm 1.59 \times 10^{-16}$ C, from 2.65×10^{-16} C to 9.75×10^{-16} C with an average of $5.34 \pm 1.76 \times 10^{-16}$ C, from 2.14×10^{-16} C to 9.03×10^{-16} C with an average of $4.81 \pm 1.40 \times 10^{-16}$ C and from 1.97×10^{-16} C to 7.34×10^{-16} C with an average of $3.94 \pm 1.26 \times 10^{-16}$ C for Hb AS, Hb AC, Hb FSC, and Hb FA respectively. The big standard deviation in the charge could be due to the variation in the size of the cells. As

we have discussed earlier, the sizes of the cells were taken into account when we determined the amplitude of the electric field of the beam acting on each cell. The size of the cells studied ranges from a $5.70\mu m$ to $9.53\mu m$ with an average diameter of $7.93 \pm 0.64\mu m$, a $6.19\mu m$ to $10.00\mu m$ with an average diameter of $7.86 \pm 1.07\mu m$, a $4.90\mu m$ to $8.90\mu m$ with an average diameter of $6.51 \pm 0.81\mu m$ and a $5.00\mu m$ to $8.49\mu m$ with an average diameter of $6.47 \pm 0.66\mu m$ for Hb AS, Hb AC, Hb FSC, and Hb FA respectively.

The results for the diameter, the charge (in z number), and charge per unit area (z number/area) for all four blood samples RBCs studied are displayed using color coded double axes Histogram in Fig. 5.6 - 5.9 of (a). In Fig 5.6 - 5.9 of (a), both the right and left vertical axes represent the number of cells but in the horizontal axes, while the top axis (colored green) represent the diameters, the bottom axis represent both the charge (in z number) (labeled in blue) and the charge per unit area (z number/area) (labeled in red). The basic statistical parameters to the Histograms for diameter (green), charge (in z number) (blue), and charge per unit area (z number/area) (red) are shown in Fig. 5.6 - 5.9 of (a) along with the hemoglobin (Hb) quantitation of four blood samples. The value of the basic statistical parameters such as diameter of the RBCs, charge (in z number) and charge per unit area (z number/area) are shown in table 5.1. The charge (in z number) and the charge per unit area (z number/area) as a function of the diameter for all four blood sample RBCs are displayed in Fig. 5.6 - 5.9 of (b) using double vertical axes following the same color codding charge per unit area (z number/area) in red and charge (in z number) in blue). The reduced data for charge (in z number) (blue), and charge per unit area (z number/area) (red) for the four blood samples RBCs are displayed in Fig. 5.6 - 5.9 of (c).

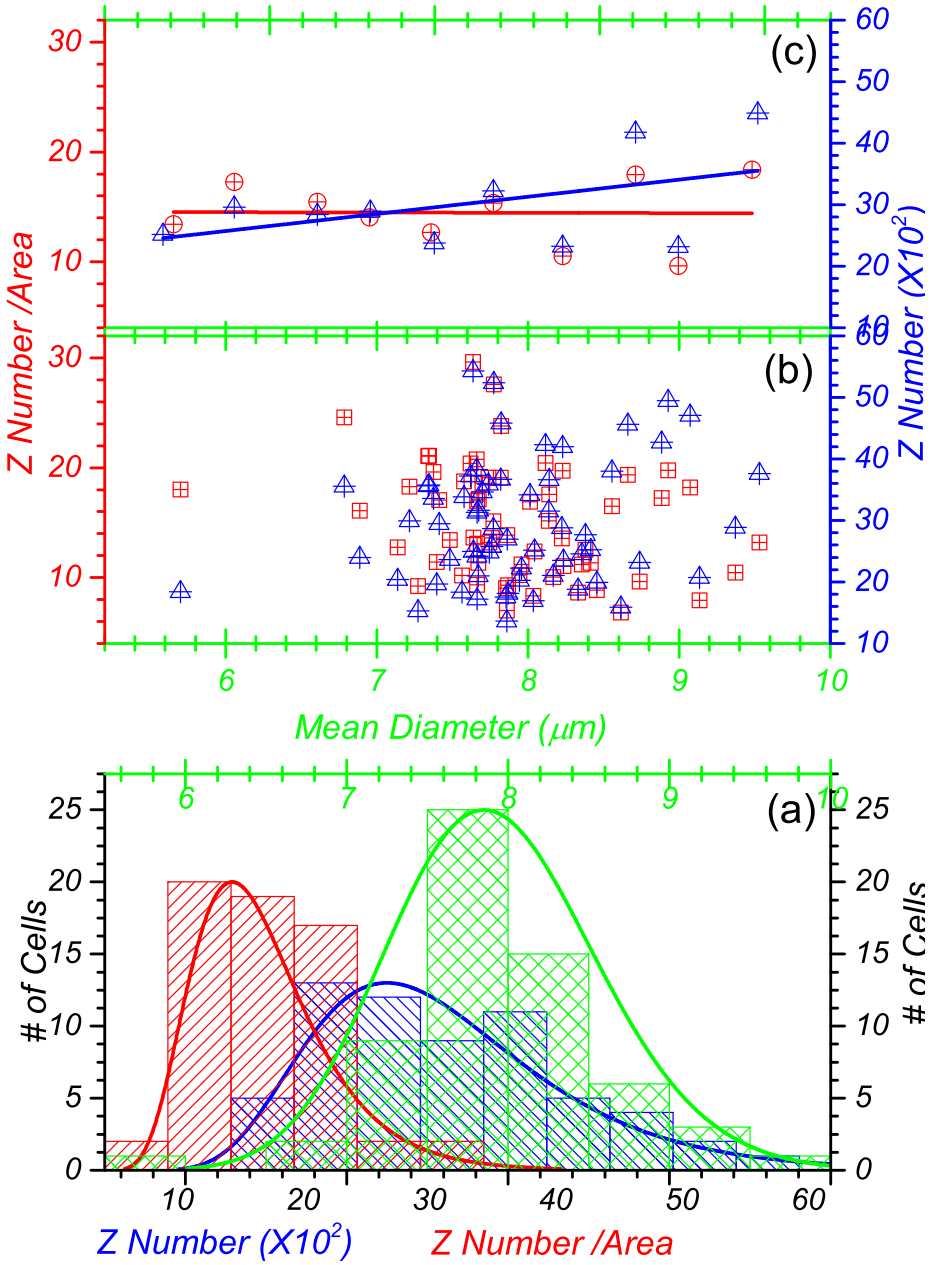

Figure 5.6: The size distribution of the graph shows that statistical distribution of the charge, charge per unit area, and the measured mean diameter of the RBCs as : (a) the statistical distribution of the mean diameter of the Hb AS blood sample (green), the charge of the Hb AS blood sample (blue), and the charge per unit area of the Hb AS blood sample (red), (b) the statistical distribution shows that the charge of the Hb AS blood sample (blue), and the charge per unit area of the Hb AS blood sample (red) as a function of the measure mean diameter for a total of 62 cells, and (c) the statistical distribution shows that the reduced data for charge of the Hb AS blood sample (blue), and the charge per unit area of the Hb AS blood sample (red) as a function of the measure mean diameter for a total 52 cells.

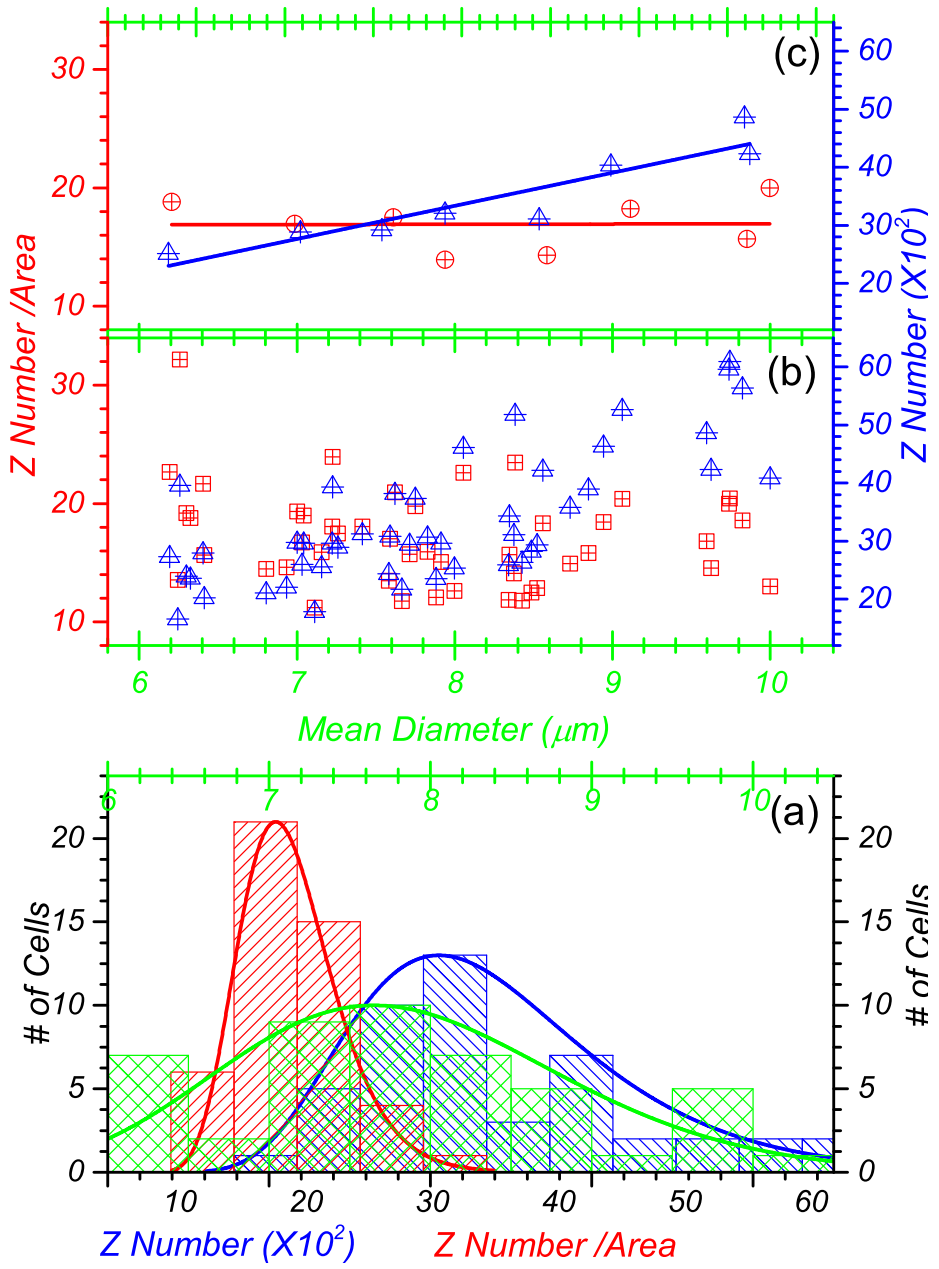

Figure 5.7: The size distribution of the graph shows that statistical distribution of the charge, charge per unit area, and the measured mean diameter of the RBCs as : (a) the statistical distribution of the mean diameter of the Hb AC blood sample (green), the charge of the Hb AC blood sample (blue), and the charge per unit area of the Hb AC blood sample (red), (b) the statistical distribution shows that the charge of the Hb AC blood sample (blue), and the charge per unit area of the Hb AC blood sample (red) as a function of the measure mean diameter for a total of 47 cells, and (c) the statistical distribution shows that the reduced data for charge of the Hb AC blood sample (blue), and the charge per unit area of the Hb AS blood sample (red) as a function of the measure mean diameter for a total 35 cells.

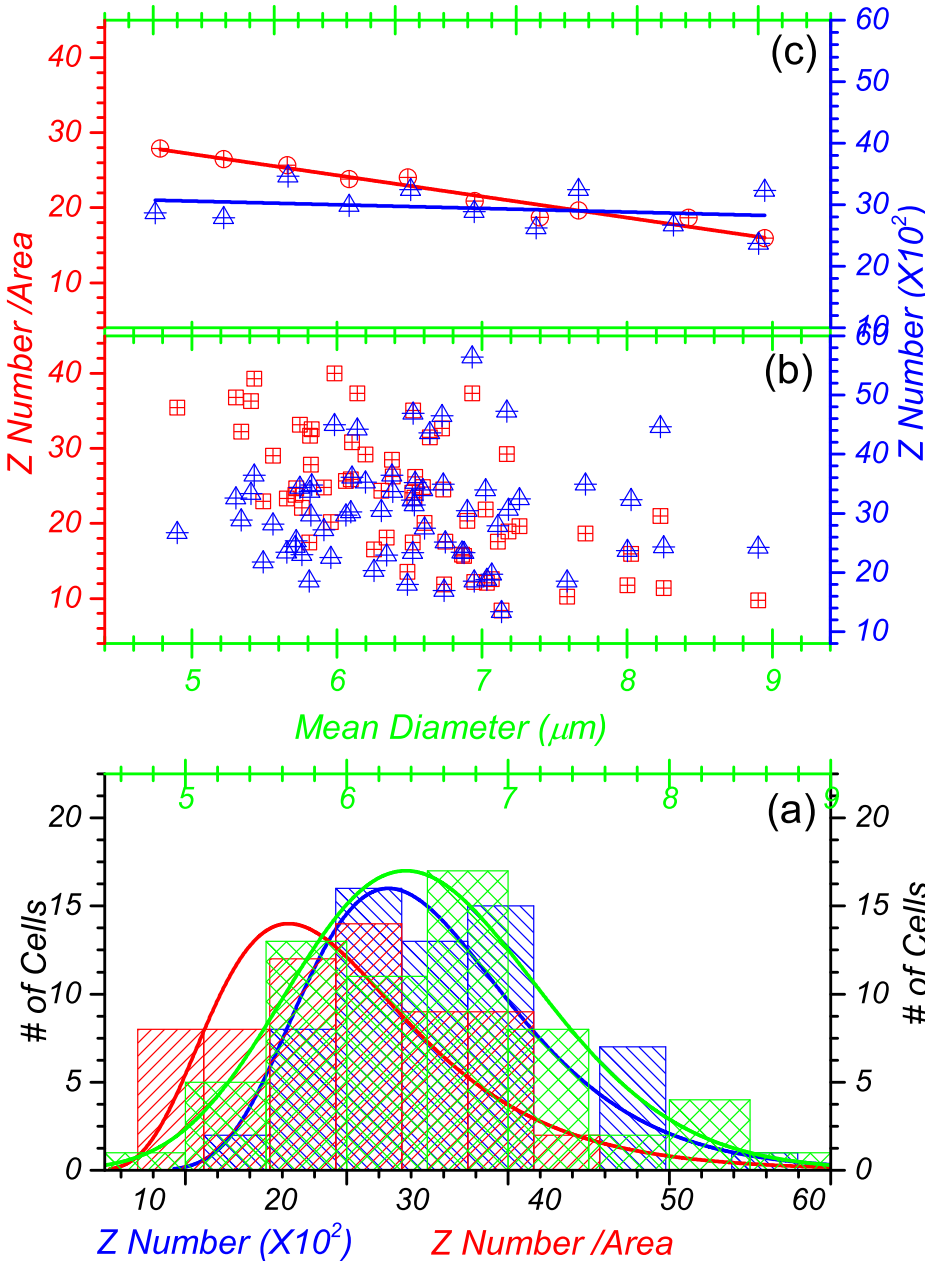

Figure 5.8: The size distribution of the graph shows that statistical distribution of the charge, charge per unit area, and the measured mean diameter of the RBCs as : (a) the statistical distribution of the mean diameter of the Hb FSC blood sample (green), the charge of the Hb FSC blood sample (blue), and the charge per unit area of the Hb FSC blood sample (red), (b) the statistical distribution shows that the charge of the Hb FSC blood sample (blue), and the charge per unit area of the Hb FSC blood sample (red) as a function of the measure mean diameter for a total of 62 cells, and (c) the statistical distribution shows that the reduced data for charge of the Hb FSC blood sample (blue), and the charge per unit area of the Hb FSC blood sample (red) as a function of the measure mean diameter for a total 52 cells.

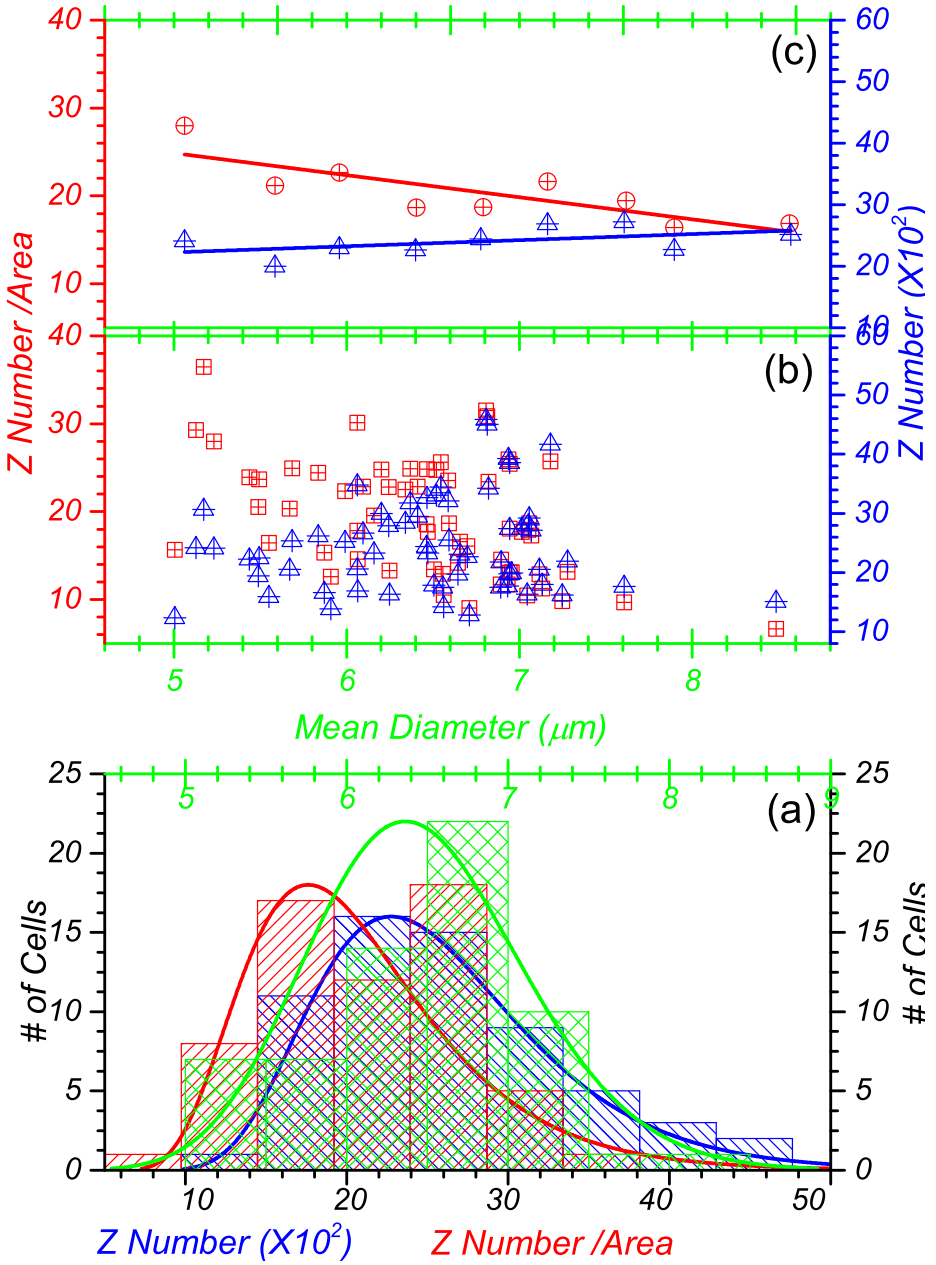

Figure 5.9: The size distribution of the graph shows that statistical distribution of the charge, charge per unit area, and the measured mean diameter of the RBCs as : (a) the statistical distribution of the mean diameter of the Hb FA blood sample (green), the charge of the Hb FA blood sample (blue), and the charge per unit area of the Hb FA blood sample (red), (b) the statistical distribution shows that the charge of the Hb FA blood sample (blue), and the charge per unit area of the Hb FA blood sample (red) as a function of the measure mean diameter for a total of 62 cells, and (c) the statistical distribution shows that the reduced data for charge of the Hb FA blood sample (blue), and the charge per unit area of the Hb FA blood sample (red) as a function of the measure mean diameter for a total 50 cells.

We have made carried out a statistically valid data reduction that would reduce the high standard deviations using graphical data analysis software, Origin Pro. 9.1. The results for the reduced data for TIE (blue) and TRD (red) are shown in Fig. 5.10 (a) and (b) respectively. In each cases the results were obtained following the same procedure. In the the first reduction, for both TIE and TRD, were made using the statistical distribution for the size measurement displayed in Fig. 5.2 - 5.5 of (a) by the green histogram. The values in first three bins (three cells with the minimum diameter) and in the last bin (three cells with maximum diameter) were eliminated from the data. In the second data reduction three cells with maximum and three cells with minimum values were eliminated for both TIE and TRD. The reduced data that consisted of a total of 50 cells were sorted out in increasing order by its diameter for Hb AS, Hb FSC, and Hb FA and 35 cells for Hb AC. The analyses is based on grouping the sorted data with increment of the bin width of the histogram for the diameter in Fig. 5.2 - 5.5 of (a). Then for each group the average values for the diameters and the corresponding TIE and TRD were calculated. These values are displayed by the blue (TIE) and red (TRD) data points in Fig. 5.10(I) (a) and (b). The corresponding best-fit line to these data points of the TRD is slightly decrease with an increase in the size of the cells, but TIE is an increase with increase in the size of the cells. Following the same procedure we have made carried out statistically valid data reduction for the charge developed (in z number) and charge per unit area are shown in Fig.5.6 - 5.9 of (a). Then for each group the average values for the diameters and the corresponding charge developed and charge per unit area were calculated. These values are displayed by the blue (charge developed) and red (charge per unit area) data points in Fig. 5.10(II) of (a) and (b). The corresponding best-fit line to these data points of the charge per unit area is independent of the size of the cells, but for charge it predicts slightly increase with increase in the size of the cells.

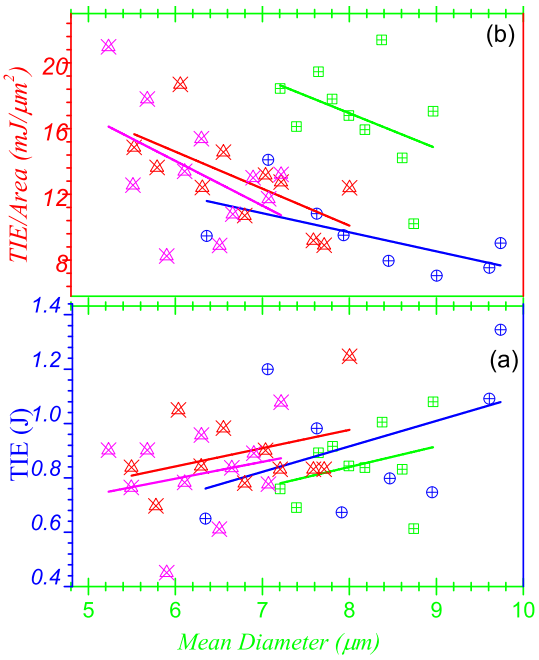

I .This graph describes the TIE (blue) and TRD (red) as a function of the diameter of the four blood sample cells green (Hb AS), blue (Hb AC), red (Hb FSC) and magenta(Hb FA).

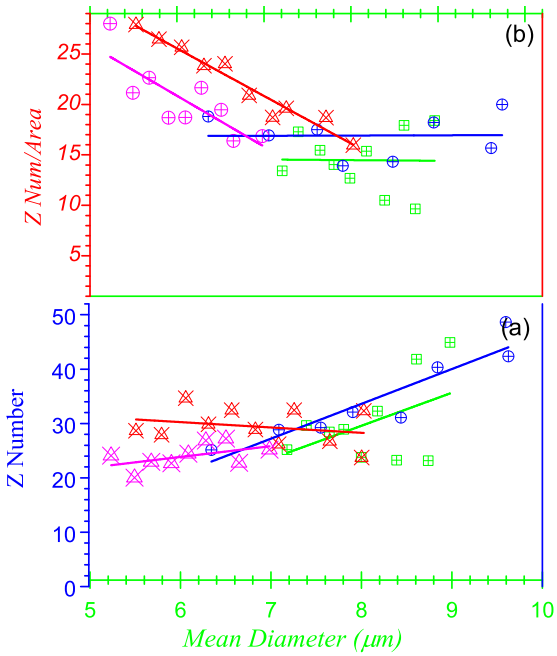

II .This graph describes the charge (blue) and charge per unit area (red) as a function of the diameter of the four blood sample cells green (Hb AS), blue(Hb AC), red (Hb FSC) and magenta (Hb FA).

Figure 5.10: The reduced statistical parameters of the TIE, TRD, charge and charge per unit area as a function of diameter of the cells of the four blood samples.

5.2 Conclusion

In this study we determined the hemoglobin quantitation, the TIE, the TRD and the charge of RBCs from four different hemoglobin types in blood samples. These blood samples are obtained from identified individuals of Hb AS, Hb AC, Hb FSC, and Hb FA. The charge to ionization energy was found as well as the ionization energy per unit mass for four samples of RBCs. This was done by creating a theoretical model based on Newtonian mechanics. The net force acting upon the cell as it was ejected from the trap was used to find the equation of motion for the cell. These forces included the electrostatic force due to the charge developed on the cell from the electric field of the laser beam, the trapping force due to the gradient of the electric field squared, and the drag force due to the viscosity of the medium through which the cell traveled. This resultant differential equation was solved after linearizing the terms using a series expansion. The solution gave an accurate model of the displacement of the cell as it was ejected from the laser trap. Parameters, such as the mass, electric field at the trap location, and the drag coefficient, were known for each cell of the four hemoglobin type in the blood samples. Thus, theoretical model was evaluated for each of the 62 cells for Hb AS, Hb FSC and Hb FA, and 47 cells for Hb AC using its specific mass, drag coefficient, and electric field. The charge developed was found specifically for each cell of the four blood samples by using a numerical nonlinear model fitting function. Which was found to be $4.72 \pm 1.59 \times 10^{-16}$ C, $5.34 \pm 1.76 \times 10^{-16}$ C, $4.81 \pm 1.40 \times 10^{-16}$ C and $3.94 \pm 1.26 \times 10^{-16}$ C for Hb AS, Hb AC, Hb FSC, and Hb FA respectively. The charge per unit area is independent of the size of the cells, but for charge it predicts slightly increase with increase in the size of the cells.

Overall, though laser trap has been used as a tool in the field of biophysics, never before has the technique been used to study the hemoglobin quantitation of RBCs in this way. The ultimate objective of this study was to find a way to understand the hemoglobin quantitation of a red blood cell and perhaps more importantly, to see a laser trap could effectively and accurately be used for this. This study demonstrated that LT technique used to determine the hemoglobin types present in a blood sample, is indeed promising. Hemoglobin quantitation in a blood sample is essential in SCD and also in monitoring patients receiving various types of

treatments.

Bibliography

[1] A. Kutlar, F. Kutlar, J. B. Wilson, M. G. Headlee, and T. H. J. Huisman, "Quantitation of hemoglobin components by high-performance cation-exchange liquid chromatography: Its use in diagnosis and in the assessment of cellular distribution of hemoglobin variants," Am. J.Hematol. **17**, 39 - 53 (1984).

[2] A. Ashkin, "Applications of laser radiation pressure," Science **210**, 1081 - 1088 (1971).

[3] A. Pellizzaro, G. Welker, D. Scott, R. Solomon, J. Cooper, A. Farone, M. Farone, R. S. Mushi, M. Aguinaga, and D. Erenso, "Direct laser trapping for measuring the behavior of transfused erythrocytes in a sickle cell anemia patient," Biomed.l Opt. Express **3**, 2190 - 2199 (2012).

[4] M. M. Brandao, A. Fontes, M. L. Barjas-Castro, L. C. Barbosa, F. F. Costa, C. L. Cesar, and S. T. Saad, "Optical tweezers for measuring red blood cell elasticity: application to the study of drug response in sickle cell disease," Eur. J. of Haemt. **70**, 207 - 211 (2003).

[5] J. C. Maxwell, Theory of Heat. Longmans, London, (1871).

[6] P.N. Lebedev, Untersuchungen ber die druckkrfte des lichtes. Ann. d. Phys. **6**, 433 (1901)

[7] E. F. Nichols, G. F. Hull, Phys. Rev. **13**, 307 (1901).

[8] A. Ashkin, J. M. Dziedzic, App.Phys.Lett. **19**, 283 (1971).

[9] A. Ashkin, J. M. Dziedzic, App.Phys.Lett. **24**, 586 (1974).

[10] A. Ashkin, J. M. Dziedzic, Science **187**, 1073 (1975).

[11] A. Ashkin, Phys. Rev. Lett. **40**, 729 (1978).

[12] A. Ashkin, Science **210**, 1081 (1980).

[13] A. Ashkin, J.M. Dziedzic, J.E. Bjorkholm, S. Chu, "Observation of a single beam gradient force optical trap for dielectric particles". Opt. Lett. **11**, 288 (1986).

[14] S. B. Smith, Y. Cui, C. Bustamante, Science **271**, 795 (1996).

[15] K. Sakata-Sogawa, M. Kurachi, K. Sogawa, Y. Fujii-Kuriyama, H. Tashiro, Eur.Biophys. J. **27**, 55 (1998).

[16] M. L. Bennink, O. D. Scharer, R. Kanaar, K. Sakata-Sogawa, J. M. Schins, J. S. Kanger, B. G. de Grooth, J. Greve, Cytometry **36**, 200 (1999).

[17] "Optical Trapping." MIT Department of Physics, (2012)

[18] A. Ashkin, "The Study of Cells By Optical Trapping and Manipulation of Living Cells Using Infrared Laser Beams," ASGSB Bulletin, **4**, 2, 133 - 146, (1991).

[19] A. Banerjee, S. Chowdhury and S. K. Gupta, "Optical Tweezers": Autonomous Robots for the Manipulation of Biological Cells, IEEE Robotics and Automation Magazine, **21**, 3, 81 - 88, (2014).

[20] Ethier C. Ross, Simmons Craig A. "Introductory Biomechanics: From Cells to Organisms." Cambridge, New York. 41-42 (2007)

[21] Neuman KC, Block SM. "Optical trapping." Review of Scientific Instruments **75**(9): 2787-2809 (2004)

[22] Y. Harada Y and T. Asakura, "Radiation Forces on a dielectric sphere in the Rayleigh Scattering Regime". Optics Communications **124**: 529 - 541 (1996)

[23] Eric M. Strohm, Eno Hysi, Michael C. Kolios, "Photoacoustic measurements of single red blood cells". IEEE International Ultrasonics Symposium Proceedings, 1406 - 1409 (2012)

[24] G. B. Liao, P. B. Bareil, Y. Sheng, and A. Chiou, "One-dimensional jumping optical tweezers for optical stretching of bi-concave human red blood cells," Opt. Express **16**(3), 1996 - 2004 (2008)

[25] M.Kelley, Y.Gao and D.Erenso, "Single cell ionization by a laser trap: a preliminary study in measuring radiation dose and charge in BT20 breast carcinoma cells," Biomedical Optics Express, **7**, 9, 3438 - 3448, (2016).

[26] C. Gary-Bobo and A. Soloman, "Hemoglobin charge dependence on hemoglobin concentration in vitro," Journal of General Physiology, **57**, 3, 283 - 289, (1971).

Declaration

This thesis is my original work, has not been presented for a degree in any other University and that all the sources of material used for the thesis have been dully acknowledged.

Signature:– – – – – – – – – – –

Place and time of submission: Addis Ababa University, June 2017

This thesis has been submitted for examination with my approval as University advisor.

Name: Prof.Daniel Erenso

Department of Physics and Astronomy, Middle Tennessee State University, Murfreesboro, Tennessee 37132, USA and Addis Ababa University

Signature:– – – – – – – – – ––